Materials Advances

Exploring a new synthesis route to lithium-excess disordered rock salt (DRX) cathode materials

Journal:	*Materials Advances*
Manuscript ID	MA-ART-12-2024-001287.R1
Article Type:	Paper
Date Submitted by the Author:	15-Mar-2025
Complete List of Authors:	Chambers, Matthew; Oak Ridge National Laboratory Physical Sciences Directorate, Chemical Sciences Li, Tianyu; UCSB, Materials Liang, Zhilin; Stanford Synchrotron Radiation Lightsource, SLAC National Accelerator Laboratory Keum, Jong; Oak Ridge National Laboratory, Neutron Scattering Division Stone, Kevin; SLAC National Accelerator Laboratory, SSRL Clément, Raphaële; University of California, Santa Barbara, Materials Research Laboratory Armstrong, Beth; Oak Ridge National Laboratory, Materials Science and Technology Division Self, Ethan; Oak Ridge National Laboratory,

Exploring a new synthesis route to lithium-excess disordered rock salt (DRX) cathode materials

Matthew S. Chambers[a]*, Tianyu Li[b], Zhilin Liang[c], Jong Keum[d,e], Kevin H Stone[c], Raphaële J. Clément[b], Beth L. Armstrong[f]*, Ethan C. Self[a]*

[a]Chemical Sciences Division, Oak Ridge National Laboratory, Oak Ridge, Tennessee 37831, United States

[b]Materials Department and Materials Research Laboratory, University of California Santa Barbara, Santa Barbara, CA 93106, USA

[c]Stanford Synchrotron Radiation Lightsource, SLAC National Accelerator Laboratory, Menlo Park, California 94025, USA

[d]Center for Nanophase Materials Sciences, Oak Ridge National Laboratory, Oak Ridge, TN 37831, USA

[e]Neutron Scattering Division, Oak Ridge National Laboratory, Oak Ridge, TN 37831, USA

[f]Materials Science and Technology Division, Oak Ridge National Laboratory, Oak Ridge, TN 37831, USA.

*Corresponding author

Abstract

Lithium-excess disordered rock salt (DRX) materials are promising candidates for Co/Ni-free Li-ion cathodes due to their high specific energy (800+ Wh kg^{-1}) and compositional flexibility. DRX cathodes are typically synthesized using solid-state reactions, which are difficult to scale and provide little-to-no control over particle morphology. To address this bottleneck, the present study reports a two-step, solution-based reaction route to prepare Mn/Ti-based DRX oxyfluoride cathodes with nominal compositions of $Li_{1.25}Mn_{0.5}Ti_{0.3}O_{1.95}F_{0.05}$ and $Li_{1.35}Mn_{0.7}Ti_{0.1}O_{1.85}F_{0.15}$. More specifically, a glycine-nitrate combustion reaction is used to produce a lithiated transition metal oxide, which is further reacted with LiF to produce high-purity DRX powders. Remarkably, this route yields 80–90% pure DRX after annealing for 1 h at 800–1000°C, and ^{19}F solid-state nuclear magnetic resonance (ssNMR) spectra demonstrate that F^- anions are successfully incorporated into the DRX structure. Cathodes prepared using this approach exhibit promising electrochemical performance, with $Li_{1.35}Mn_{0.7}Ti_{0.1}O_{1.85}F_{0.15}$ attaining reversible capacities ~210 mAh g^{-1} and moderate cycling stability in half cells (65% capacity retention over 150 cycles). Overall, these results demonstrate that utilizing novel metal oxide precursors presents a viable and largely unexplored method to produce high-performance Co/Ni-free DRX cathodes.

Introduction

Lithium-ion batteries (LIBs) are ubiquitous in a wide range of applications including portable electronics, electric vehicles, and grid storage. The cost and energy density of LIBs are largely influenced by the cathode active material. State-of-the-art layered oxides such as $LiNi_xMn_yCo_{1-x-y}O_2$ (NMC) and $LiNi_xCo_yAl_{1-x-y}O_2$ (NCA) have high operating voltages >3.8 V vs. Li/Li^+ and reversible capacities up to ~220 mAh g^{-1}, but their over-reliance on Ni and Co presents challenges in developing sustainable supply chains. Co/Ni-free alternatives, including olivine $LiFePO_4$[1] and spinel $LiMn_2O_4$,[2-6] have been commercialized, although these materials have significantly lower energy density than most layered oxides. Such limitations highlight the need for new cathode active materials based on earth-abundant transition metals.

Li-excess disordered rock salt (DRX) oxides represent a promising class of next-generation Li-ion cathodes.[7-15] DRX materials adopt the cubic *Fm*-3*m* rock salt structure, where Li^+ and transition metals occupy the cation site, and O^{2-} anions occupy the anion site. Typically, these materials contain both redox-active transition metal(s) (*e.g.*, Mn and Ni) and d^0 transition metal(s) (*e.g.*, Ti^{4+}, Zr^{4+}, and Nb^{5+}),[7, 8, 16] where the latter stabilizes the DRX structure.[17] Compared to conventional Li-ion cathodes, DRX materials exhibit broad compositional flexibility, and their disordered nature may provide other advantages, including smaller volume changes during cycling.[9] DRX cathodes reported in the literature have shown impressive performance including specific capacities ≥ 300 mAh g^{-1} and specific energies ~1000 W h kg^{-1}.[18, 19] Their electrochemical performance can be further improved by partially substituting O^{2-} with F^-, which has been widely investigated for Mn/Ti-based compositions (*e.g.*, $Li_{1+x}Mn_yTi_{1-x-y}O_{2-z}F_z$).[10, 13, 18, 20-26] In addition to improving oxidative stability, F^- substitution has been shown to increase Li^+ mobility *via* formation of percolating 0-TM channels in $Li_{1.2}Ti_{0.35}Ni_{0.35}Nb_{0.1}O_{1.8}F_{0.2}$.[27] Ouyang *et al*.[28] showed that fluorination levels < 10% (*i.e*. 0.2 mol F per DRX formula unit) hinder Li^+ percolation compared to the pure oxide DRX, but Li^+ mobility increases at higher fluorination levels (>15%). Recent work by Wu *et al.* demonstrated that

the performance of Mn-rich DRX cathodes ($Li_{1+x}Mn_yTi_{1-x-y}O_{2-z}F_z$, $y \geq 0.5$) primarily depends on the Mn content, while fluorination plays a secondary role.[26]

Despite their promising attributes, a major limitation of DRX cathodes is the lack of flexible synthesis platforms, which are needed to fine-tune the material's structure and performance. DRX powders are typically prepared using solid-state methods, which utilize ball milling to mix inorganic precursors followed by high-temperature reactions (*e.g.*, 12 h at 1000 °C[10] or > 9 h at ≥ 900 °C).[7] These methods are difficult to scale and provide little control over particle morphology. For oxyfluoride compositions, this lack of control is compounded by uncertainty in the product's stoichiometry due to LiF evaporation at high temperature (T_m = 848 °C for LiF)[29] and/or the presence residual amorphous LiF in the final product, which cannot be detected using standard scattering tools.[10] Furthermore, preparing Mn-rich compositions ($y \geq 0.5$ in $Li_{1+x}Mn_yTi_{1-x-y}O_{2-z}F_z$) is challenging due to the high energy of Mn–F bonds compared to Li–F and Ti–F bonds.[30] For example, Szymanski *et al*. reported difficulty in simultaneously incorporating Mn^{3+} and F^- into the DRX lattice when using Li_3TiO_3F and MnO precursors.[10] Considering these challenges, alternative methods have been explored to produce DRX cathodes including mechanochemical,[20, 21, 23] sol-gel,[7] molten salt,[31] and microwave synthesis routes.[15] Intriguingly, some reports have shown that using LiF as a fluorinating agent facilitates DRX phase formation.[15, 20]

Combustion synthesis represents a scalable route that has not yet been explored for DRX cathodes. This approach, which has been widely employed for solid-oxide fuel cell materials[32-37] and Li-ion cathodes (e.g., Li_2MnO_3[38] Mn-doped $LiFePO_4$[39], and Mn-based spinels[40, 41]), enables the production of powders with precise compositional control and complex chemistries that are not accessible through traditional routes. The method is also used in industrial processes such as production of yttria-stabilized zirconia[42] and $La_{1-x}Sr_xMnO_3$.[37] In combustion reactions, an aqueous solution containing metal precursors, oxidizing agents (*e.g.*, nitrate salts[32-37, 43-45]), and a fuel (*e.g.*, malic acid,[43] sucrose,[44] citric acid,[33, 36] cellulose,[33] ethylene glycol[36] or glycine[32, 35, 45]) is heated to its autoignition temperature, resulting in the rapid production of nanocrystalline oxide powders. Compared to solid-state and molten-salt synthesis routes which are

generally limited to gram-scale quantities, combustion reactions offer several advantages including: (i) atomic mixing of precursors in solutions, which can be readily scaled to yield kg+ batches, (ii) modest reaction temperatures (300 – 400 °C) to initiate the self-propagating exothermic reactions, and (iii) the ability to produce powders with controlled particle morphology.[42] Thus, combustion reactions present an opportunity to address critical synthesis challenges for DRX cathodes.

The present study reports the synthesis and characterization of Mn/Ti-based DRX oxyfluoride cathodes prepared through a two-step route involving: (i) a combustion reaction to prepare a lithiated transition metal oxide precursor, followed by (ii) a high-temperature, solid-state reaction with LiF to produce the final DRX powder. This method is demonstrated for cathodes with two different Mn contents including $Li_{1.25}Mn_{0.5}Ti_{0.3}O_{1.95}F_{0.05}$ and $Li_{1.35}Mn_{0.7}Ti_{0.1}O_{1.85}F_{0.15}$. Overall, the approach yields up to ~90% pure DRX powders which can be prepared at lower temperatures and over shorter timeframes (*e.g.*, 800 °C and 1 h) compared to conventional solid-state processes (*e.g.*, ball milling for 16 h followed by heating at 1100 °C for 2 h[16] or ball milling for 6 h followed by heating at 800 °C for 12 h[29]). Notably, producing pure DRX oxides is difficult with this solution-based route, and adding LiF to the oxide precursor is critical to facilitate DRX phase formation during the second heating step. This work provides a detailed analysis of the reaction pathway and product's structure using *in-situ* and *ex-situ* X-ray diffraction (XRD). These findings are complemented by other characterization methods including: (i) solid-state nuclear magnetic resonance (ssNMR) spectroscopy to probe the distribution of local Li and F environments, (ii) scanning electron microscopy (SEM) to assess particle morphology, and (iii) inductively-coupled plasma optical emission spectroscopy (ICP-OES) and fluoride ion-selective electrode analysis (F-ISE) to determine precise stoichiometries of the fluorinated powders. The reported Mn/Ti-based DRX cathodes exhibit promising electrochemical performance, with $Li_{1.35}Mn_{0.7}Ti_{0.1}O_{1.85}F_{0.15}$. attaining stable capacities up to ~210 mAh g^{-1} in Li metal half cells. Overall, these results illustrate the merits and opportunities for scalable combustion reactions to produce DRX cathodes.

Experimental Procedures

Precursor Synthesis

Oxide precursors with nominal compositions of $Li_{1.2}Mn_{0.5}Ti_{0.3}O_{1.95}$ and $Li_{1.2}Mn_{0.7}Ti_{0.1}O_{1.85}$ were synthesized *via* combustion reactions. In this process, stoichiometric amounts of Mn nitrate, Li nitrate, and Tyzor® were mixed to form a single solution. Glycine was dissolved in the precursor solution using a stoichiometric glycine-nitrate ratio,[46] which was calculated assuming that: (i) the only gaseous by-products are H_2O, CO_2, and N_2 and (ii) all nitrates and glycine are consumed in the reaction. The solution was heated on a hot plate to 350 °C in air, initially producing a white foam and releasing NO_x species before combusting to form a black solid. The resulting solid was ground with a ceramic mortar and pestle and heated in a muffle furnace at 300 °C for 2–4 h in air (heating and cooling rates of ±10 °C min^{-1}), after which the sample was ground again and stored in a desiccator. The combustion reactions yielded approximately 10 g of precursor material.

Safety Note: Due to the release of NO_x species, the combustion reaction should be performed inside a fume hood. This reaction produces nanocrystalline powders, which may be present as nanoparticles. Therefore, the fume hood should also be suitable for nanomaterials.

DRX Synthesis

Annealed oxide powders with nominal compositions of $Li_{1.2}Mn_{0.5}Ti_{0.3}O_{1.95}$ and $Li_{1.2}Mn_{0.7}Ti_{0.1}O_{1.85}$ were prepared by heating the precursors to 1000 °C under flowing Ar for 4 and 1 h, respectively, (heating/cooling rates of ±5 °C min^{-1}). While optimizing the synthesis conditions for $Li_{1.2}Mn_{0.5}Ti_{0.3}O_{1.95}$ and $Li_{1.25}Mn_{0.5}Ti_{0.3}O_{1.95}F_{0.05}$, it was determined that annealing at 1000°C for 4 h decreased the DRX phase conversion, and thus a 1 h dwell time was used for subsequent reactions. A third oxide powder with the nominal composition $Li_{1.25}Mn_{0.5}Ti_{0.3}O_{1.975}$ was synthesized by reacting the precursor with Li_2O (Thermo Fisher Scientific, 99.5%) at 1000 °C for 1 h (heating/cooling rates of ±5 °C min^{-1}) based on the following reaction:

$$Li_{1.2}Mn_{0.5}Ti_{0.3}O_{1.95} + 0.025Li_2O \rightarrow Li_{1.25}Mn_{0.5}Ti_{0.3}O_{1.975}. \quad \text{Equation 1}$$

DRX oxyfluorides with nominal compositions of $Li_{1.25}Mn_{0.5}Ti_{0.3}O_{1.95}F_{0.05}$ and $Li_{1.35}Mn_{0.7}Ti_{0.1}O_{1.85}F_{0.15}$ were synthesized by grinding the oxide precursors with stoichiometric amounts of LiF (Alfa Aesar, 99.8%) and heating to 800 – 1000 °C under flowing Ar for 1–4 h (heating/cooling rates of ±5 °C min^{-1}) to yield ~0.6 g of final product. During the initial set of reactions, precursors were ground with LiF in air. However, as the precursors are hygroscopic, a second set of reactions was performed by grinding the precursors (dried at 90°C under vacuum for 24 h) with LiF in an Ar-filled glove box with low H_2O content (<10 ppm). Both approaches yielded similar cathode phase purity, morphology, and electrochemical performance. A summary of all reaction conditions investigated in this study is provided in Table S2. The compositions of select samples were determined using ICP-OES and F-ISE measurements performed by Galbraith Laboratories Inc.

Li_3TiO_3F Synthesis

To confirm the assignment of an impurity peak in the ^{19}F ssNMR spectrum for $Li_{1.25}Mn_{0.5}Ti_{0.3}O_{1.95}F_{0.05}$, Li_3TiO_3F was synthesized *via* a solid-state route. Stoichiometric amounts of Li_2CO_3 (Sigma, 99.99%), TiO_2 (Sigma, 99.99%), and LiF (Sigma, 99.99%) were intimately mixed using a mortar and pestle and pressed into a pellet (10 mm diameter). The pellet was calcined at 800 °C for 24 h. The sample was quenched by removing the pellet from the furnace at 800 °C and subsequently hand-ground for characterization.

X-ray Diffraction (XRD)

Ex-situ XRD was performed using a Rigaku SmartLab with a HyPix-3000 detector set in horizontal mode measuring with Bragg-Brentano geometry and either a Mo or Cu radiation source. Measurements with the Mo source (2:1 $K\alpha_1$:$K\alpha_2$; λ_1 = 0.70930 Å; λ_2 = 0.71359 Å) were collected with a $\theta/2\theta$ range of 5 – 65° and a scan rate of 1.5° min^{-1}. Measurements with the Cu source (2:1 $K\alpha_1$:$K\alpha_2$; λ_1 = 1.54056 Å; λ_2 = 1.54439 Å) were collected with a $\theta/2\theta$ range of 10 – 90° and a scan rate of 1.5° min^{-1}. The dried $Li_{1.2}Mn_{0.5}Ti_{0.3}O_{1.95}$ and $Li_{1.2}Mn_{0.7}Ti_{0.1}O_{1.85}$ precursors were measured using an air-tight sample holder which

was loaded inside an Ar-filled glove box. All other powders were loaded in air onto glass sample holders. *Ex-situ* XRD data for Li_3TiO_3F were acquired on a Panalytical Empyrean with a Cu radiation source (2:1 $K\alpha_1$:$K\alpha_2$) using a $\theta/2\theta$ range of 10 – 90° and a scan rate of 0.2° min^{-1}.

In-situ XRD data were collected using a Panalytical Xpert with a Cu radiation source (2:1 $K\alpha_1$:$K\alpha_2$) with a $\theta/2\theta$ range of 10 – 90° and a scan rate of 1.5° min^{-1} at each temperature. For these measurements, $Li_{1.2}Mn_{0.5}Ti_{0.3}O_{1.95}$ was ground with LiF in an Ar-filled glove box, and the sample was heated under flowing Ar using an Anton Paar XRK-900 furnace. The powder was loaded onto the sample holder in air. Data were collected at 27 °C, and incrementally every 100 °C from 100 – 800 °C at a ramp rate of 10 °C min^{-1}. The sample was left to equilibrate for 3 minutes before each measurement.

Rietveld Analysis

Rietveld refinements[47] were performed against *ex-situ* and *in-situ* XRD data using TOPAS-Academic v7[48] to determine phase composition. Cell parameters for each phase were refined with symmetry constraints. A single isotropic atomic displacement parameter was used for each phase. The background was modelled using a 12-fold Chebyshev polynomial, and peak shapes were modelled using a Thompson-Hastings-Cox pseudo-Voigt function. The DRX phase was modelled using the compositions $Li_{1.2}Mn_{0.4}Ti_{0.4}O_2$ and $Li_{1.1}Mn_{0.8}Ti_{0.1}O_2$ for the low-Mn and Mn-rich phases, respectively. Atomic occupancies were not refined. The starting models used for secondary phases are given in Table S1. For $Li_{1.25}Mn_{0.5}Ti_{0.3}O_{1.95}F_{0.05}$ and $Li_{1.35}Mn_{0.7}Ti_{0.1}O_{1.85}F_{0.15}$, the monoclinic rock salt phase (m-Rock Salt) was modeled using Li_2TiO_3 (space group: $C2/c$)[49] and Li_2MnO_3 (space group: $C2/m$),[50] respectively. $LiMnO_2$ (space group: $Pmmm$)[51] was used to model the orthorhombic rock salt (o-Rock Salt) phase for both compositions. For *in-situ* experiments, 4 – 5 secondary phases were included to obtain weight percentages at each temperature. For the precursors, a 4-fold spherical harmonic function was applied to model preferred orientation observed in $LiNO_3$.

Solid-State Nuclear Magnetic Resonance (ssNMR) Spectroscopy

As-synthesized $Li_{1.2}Mn_{0.5}Ti_{0.3}O_{1.95}F_{0.05}$ and $Li_{1.2}Mn_{0.7}Ti_{0.1}O_{1.85}F_{0.15}$ samples were analyzed using ^{7}Li and ^{19}F ssNMR spectroscopy to evaluate the distributions of Li and F local environments. ^{7}Li and ^{19}F ssNMR spectra were acquired using a wide bore Bruker BioSpin spectrometer charged to 2.35 T (100 MHz for ^{1}H) and equipped with a DMX 500 MHz console and a custom-made 1.3 mm, single channel broadband magic-angle spinning (MAS) probe tuned to either ^{7}Li (38.9 MHz) or ^{19}F (94.1 MHz). Spectra were obtained using a rotor-synchronized spin-echo sequence ($90° - \tau_R - 180° - \tau_R$) using a 90° radio frequency pulse of 0.45 μs for ^{7}Li and of 0.3 μs for ^{19}F. ^{7}Li chemical shifts were externally referenced against a 1 M aqueous LiCl solution (δ_{iso} = 0 ppm). ^{19}F chemical shifts were referenced against a 1 M aqueous NaF (^{19}F $\delta_{iso} = -118.14$ ppm) solution. A long recycle delay of 20 s was used for ^{7}Li ssNMR acquisitions to ensure that all ^{7}Li spins in the sample re-equilibrated between scans. For ^{19}F ssNMR, a first acquisition was conducted using a short recycle delay of 20 ms to maximize the signal from paramagnetic F environments in the DRX structure, and a second acquisition was conducted using a long recycle delay of 20 s to obtain a quantitative measurement of the diamagnetic F species within each sample. Samples were loaded into NMR rotors in an Ar-filled glovebox, and the rotors were spun at 60 kHz MAS using dry nitrogen during data acquisition. The NMR data was processed using the Bruker TopSpin 3.6.0 software.

Scanning Electron Microscopy (SEM)

SEM was performed on a Zeiss MERLIN electron microscope operating at an accelerating voltage of 1.0 kV. Prior to measurements, powder samples were ground with a mortar and pestle and adhered to the sample stub using carbon tape.

Electrochemical Characterization

The electrochemical performance of DRX oxyfluorides was evaluated in composite slurry-cast cathodes. A 78:22 w:w mixture containing DRX and graphite (MSE Supplies, TIMCAL KS-6) powders

was milled in a Spex® 8000M using a stainless steel jar with 5 mm stainless steel media (mass ratio of 10:1 media:powder) for 1 h following the procedure described elsewhere.[7] The DRX/graphite mixture was then blended with *N*-methyl-2-pyrrolidone (NMP; Sigma, 99.5%) and a polyvinylidene fluoride (PVDF, Kynar) binder solution (10 wt% in NMP) in a polypropylene vial on a Turbula T2F mixer for 1 h. The slurry was cast onto a C-coated aluminum current collector using a doctor blade (wet gap 200 μm). The electrode laminates were dried in air on a hot plate at 100 °C for 2 hours. Cathode disks (7/16" diameter) were punched and dried under vacuum at 90 °C overnight and transferred to an Ar-filled glove box. The final electrodes contained DRX/graphite/PVDF in a 70/20/10 weight ratio and had areal loadings of approximately 2 mg_{DRX} cm^{-2}. Flooded R2032 cells containing the DRX cathode, Celgard 2325 separator, liquid electrolyte [1.2 M $LiPF_6$ in 3:7 w:w ethylene carbonate:ethyl methyl carbonate (SoulBrain MI)], and Li metal auxiliary/reference electrode (0.75 mm thick disc) were prepared in the glovebox. Electrochemical performance was evaluated on a Maccor 4000 battery cycler by polarizing the cathodes between 2.0 – 4.8 V vs. Li/Li^+ at specific currents of 10 mA g^{-1} for the first 5 cycles followed by 20 mA g^{-1} for subsequent cycles. All specific capacities reported herein are normalized to the active material's mass.

Results and Discussion

The central goal of this study was to use scalable combustion reactions to prepare DRX oxide/oxyfluoride powders. Two oxide precursors (nominal compositions of $Li_{1.2}Mn_{0.5}Ti_{0.3}O_{1.95}$ and $Li_{1.2}Mn_{0.7}Ti_{0.1}O_{1.85}$) were synthesized using the glycine-nitrate process described in the experimental procedures. These compositions were designed with 2.5–7.5% anion vacancies assuming complete conversion to a DRX phase. To demonstrate proof-of-concept, the present study produced precursors in ~10 g batches, and these solution-based reactions can be easily scaled to produce kg quantities.[52] After the combustion reaction, three different heat treatment pathways were investigated to form the final product (see Schematic 1). In addition to heating the as-obtained oxide precursor alone (Path A), the material was also ground with either Li_2O or LiF prior to heating (Paths B and C, respectively).

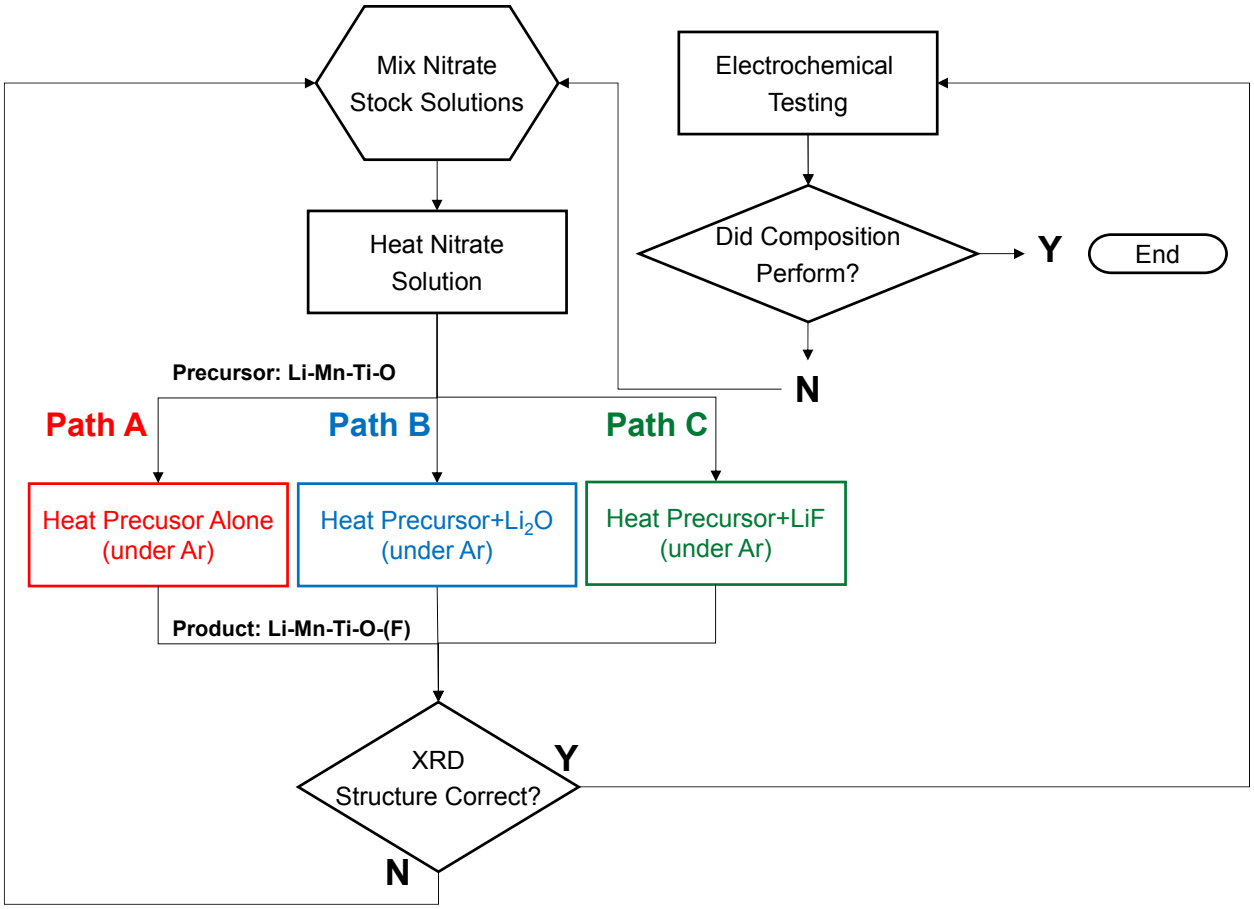

Schematic 1 – Flow diagram of the combustion synthesis route used in this study.

$Li_{1.2}Mn_{0.5}Ti_{0.3}O_{1.95}$ and $Li_{1.25}Mn_{0.5}Ti_{0.3}O_{1.975}$ Oxide Synthesis

As shown in Figure 1a, heating the $Li_{1.2}Mn_{0.5}Ti_{0.3}O_{1.95}$ precursor at 1000 °C for 4 h (Schematic 1 Path A) yielded a powder with only 47.6(8)% DRX and a large amount of secondary phases including a monoclinic rock salt (m-Rock Salt, 45.9(8)%) and $LiMn_2O_4$ spinel (6.5(5)%) . It should be noted that Mn^{3+}, Mn^{4+} and Ti^{4+} cannot be distinguished with XRD due to their similar form factors. As such, the monoclinic phase could be present as Li_2TiO_3, Li_2MnO_3 or $Li_2Ti_{1-x}Mn_xO_3$. To mitigate possible Li loss during annealing, a second synthesis attempt involved grinding the precursor with Li_2O prior to heating (see

Schematic 1 Path B and Equation 1). As shown in Figure 1b, the resulting product contained similar amounts of monoclinic rock salt (42.6(7)%) and spinel (4.3(3)%) phases.

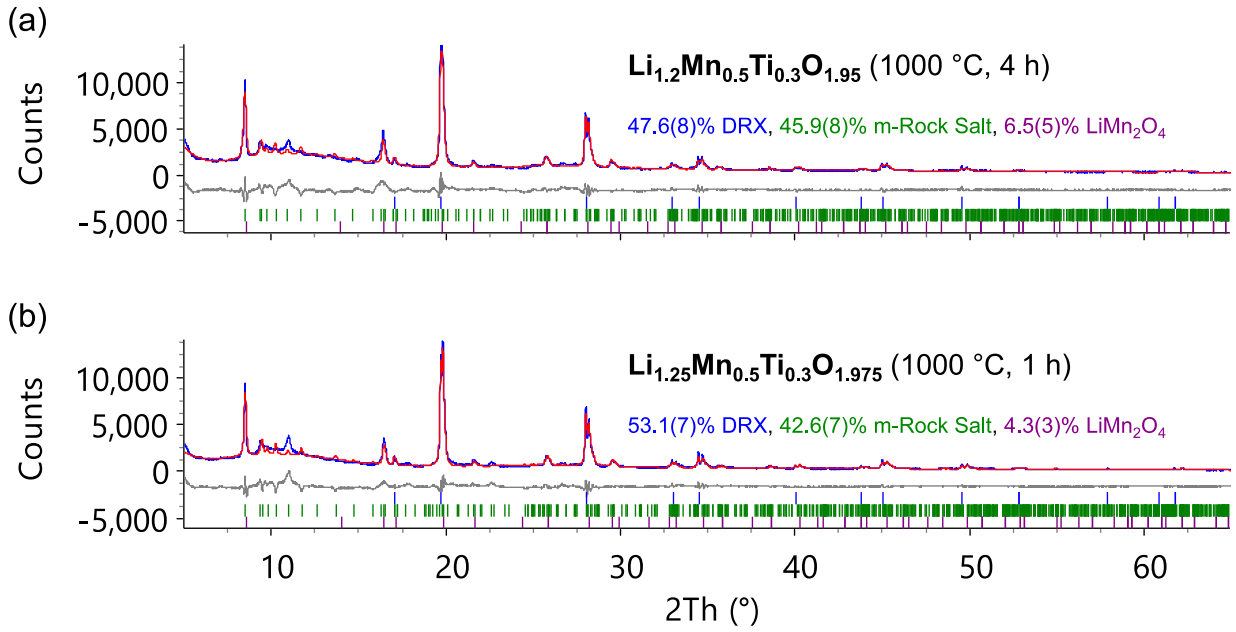

Figure 1 – Rietveld plots (Mo radiation) for products obtained by: (a) heating the $Li_{1.2}Mn_{0.5}Ti_{0.3}O_{1.95}$ precursor alone (Schematic 1, Path A), R_{wp} = 10.644%, χ^2 = 3.615 and (b) heating $Li_{1.2}Mn_{0.5}Ti_{0.3}O_{1.95}$ + 0.025Li_2O (Schematic 1, Path B), R_{wp} = 13.465%, χ^2 = 3.967. Blue curves = observed data; red curves = calculated patterns; grey curves = difference between observed and calculated data. Tick marks correspond to reflections arising from each phase. m-Rock Salt and o-Rock Salt refer to monoclinic and orthorhombic rock salt phases, respectively.

$Li_{1.25}Mn_{0.5}Ti_{0.3}O_{1.95}F_{0.5}$ Oxyfluoride Synthesis

As attempts to synthesize DRX oxides were unsuccessful, additional reactions were performed to assess the effects of F^- substitution on the final product's structure and phase purity. Here, LiF was mixed with the $Li_{1.2}Mn_{0.5}Ti_{0.3}O_{1.95}$ precursor prior to the high-temperature reaction as shown in Schematic 1 Path C and described by Equation 2:

$$Li_{1.2}Mn_{0.5}Ti_{0.3}O_{1.95} + 0.05LiF \rightarrow Li_{1.25}Mn_{0.5}Ti_{0.3}O_{1.95}F_{0.05} \quad \text{(Equation 2)}$$

Heating this mixture to 1000°C for 1 h yielded a product with 94.1(2)% DRX, 3.25(18)% monoclinic rock salt, and 2.70(13)% $LiMn_2O_4$ spinel (Figure 2a). Comparing these results with Figure 1a demonstrates that adding LiF to the precursor greatly facilitates DRX phase formation. Similarly, heating at 800 °C for 1 h yielded 86.4(3)% DRX, 12.1(6)% monoclinic rock salt, and 1.56(16)% orthorhombic rock salt (o-Rock Salt, see Figure 2b) The beneficial impact of a small amount of LiF on the final product's purity has also been reported for mechanochemical[20] and microwave[15] synthesis routes. Two plausible mechanisms for the improved phase conversion of DRX oxyfluorides include: (i) LiF serving as a sintering agent and/or (ii) F^- substitution in the DRX lattice altering the reaction pathway and energy landscape. While quantifying the relative importance of each mechanism is difficult, the present dataset suggests the latter may dominate. More specifically, NMR and F-ISE measurements (discussed below) demonstrate that F^- is successfully doped into the DRX structure rather than precipitating out as a secondary phase (e.g., LiF) at grain boundaries. More detailed investigations on the role of LiF would require *in-situ* neutron and X-ray total scattering methods combined with computational modeling to probe how the Li^+ and F^- environments evolve during the reaction. Such measurements are outside the focus of the present work but are recommended for future studies on DRX oxyfluorides.

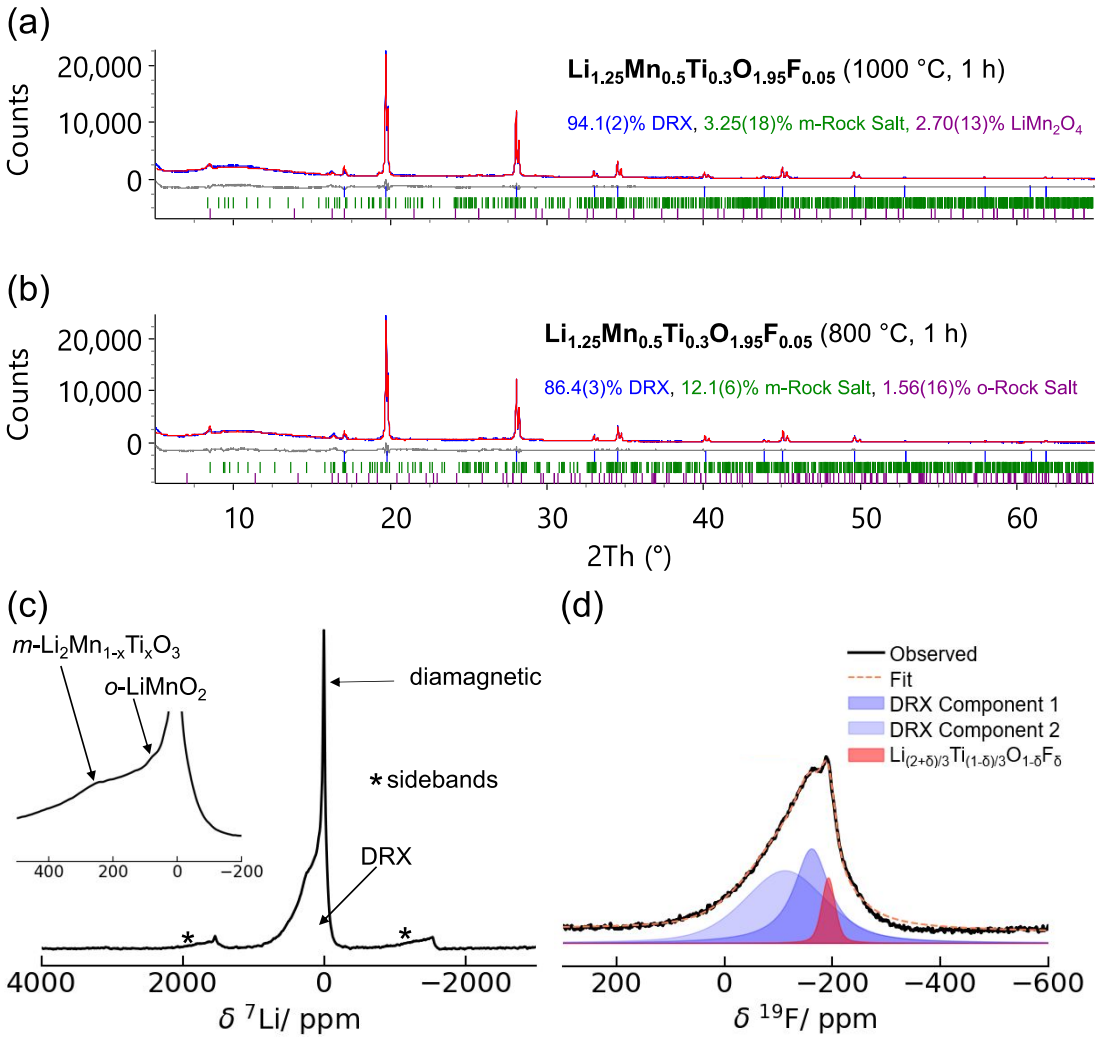

Figure 2 – (a–b) Rietveld plots (Mo radiation) for $Li_{1.25}Mn_{0.5}Ti_{0.3}O_{1.95}F_{0.05}$ synthesized at (a) 1000 °C for 1 h, R_{wp} = 9.779%, χ^2 = 2.835 and (b) 800 °C for 1 h, R_{wp} = 9.349%, χ^2 = 2.760. Blue curves = observed data, red curves = calculated pattern, grey curves = difference between observed and calculated. Tick marks correspond to reflections arising from each phase. m-Rock Salt and o-Rock Salt refer to monoclinic and orthorhombic rock salt phases, respectively. (c–d) ssNMR results for $Li_{1.25}Mn_{0.5}Ti_{0.3}O_{1.95}F_{0.05}$ heated at 800 °C for 1 h including (c) ^{7}Li (D1 = 20 s) and (d) ^{19}F (D1 = 20 ms) spectra. The inset in (c) highlights shoulders at 36 ppm and 240ppm. The peak deconvolution in (d) shows a sharp component at -196 ppm, which is similar to that of Li_3TiO_3F (see Figure Sc), and the broad signal is fit with two arbitrary DRX components. Sidebands are denoted with asterisks (*). Side bands were not plotted in (d) as they do not appear in the given chemical shift range. NMR spectra were taken under 100 MHz field at 40 kHz MAS.

To further probe the reaction between the $Li_{1.2}Mn_{0.5}Ti_{0.3}O_{1.95}$ precursor and LiF, *in-situ* XRD experiments were performed (Figure 3). The starting precursor contains nanocrystalline Mn_2O_3 and $LiMn_2O_4$, with sharp Bragg reflections arising from unreacted $LiNO_3$ (see Figure S1a). Rietveld refinements were performed for data acquired between 300 and 800°C (Figure 4). At 300 °C (Figure 4a), peaks associated with $LiNO_3$ disappear due to melting of this phase, and the sample contains primarily $LiMn_2O_4$ (43.4(16)%) and Mn_2O_3 (24.6(12)%). At 500 °C (Figure 4b), the dominant phase is a monoclinic rock salt, which accounts for 45(3)% of the sample. The DRX phase may also begin forming at this stage, as the weight percentage obtained from Rietveld refinement is 30(2)%. However, it should be noted that the peaks are very broad at this temperature, resulting in significant overlap between reflections associated with the DRX, monoclinic rock salt, and $LiMn_2O_4$ phases. At 700 °C (Figure 4c), the DRX phase is clearly present, with a weight percentage of 38(2)%. At 800 °C (Figure 4d), the dominant phase is DRX (76.8(13)%), which is in good agreement with the *ex-situ* results shown in Figure 2b.

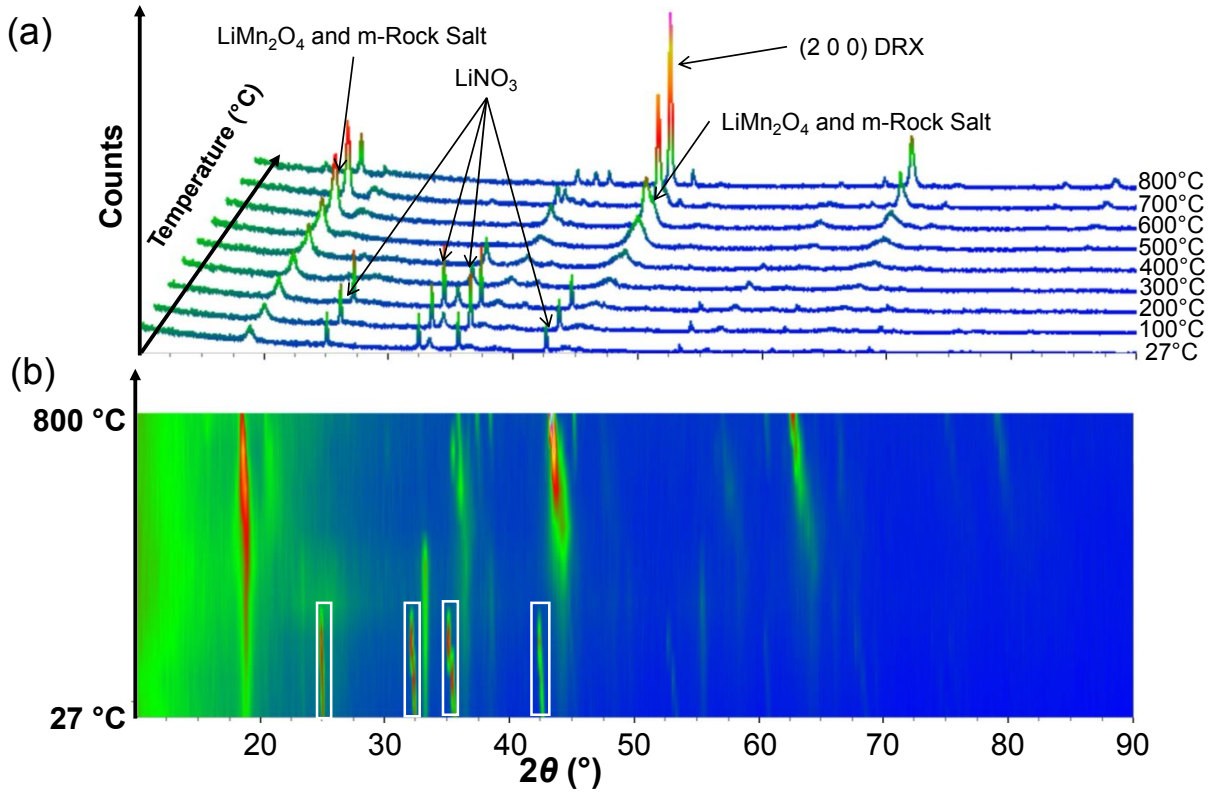

Figure 3 –XRD patterns (Cu radiation) of the *in-situ* reaction to produce $Li_{1.25}Mn_{0.5}Ti_{0.3}O_{1.95}F_{0.05}$ (Equation 2). (a) 3D plot highlighting notable peaks and corresponding phases and (b) surface plot where peaks arising from unreacted $LiNO_3$ in the precursor are denoted by white boxes. Data were collected at 27 °C, and incrementally every 100 °C from 100 – 800 °C at a ramp rate of 10 °C min^{-1}. The sample was left to equilibrate for 3 minutes before each measurement. m-Rock Salt refers to a monoclinic rock salt phase.

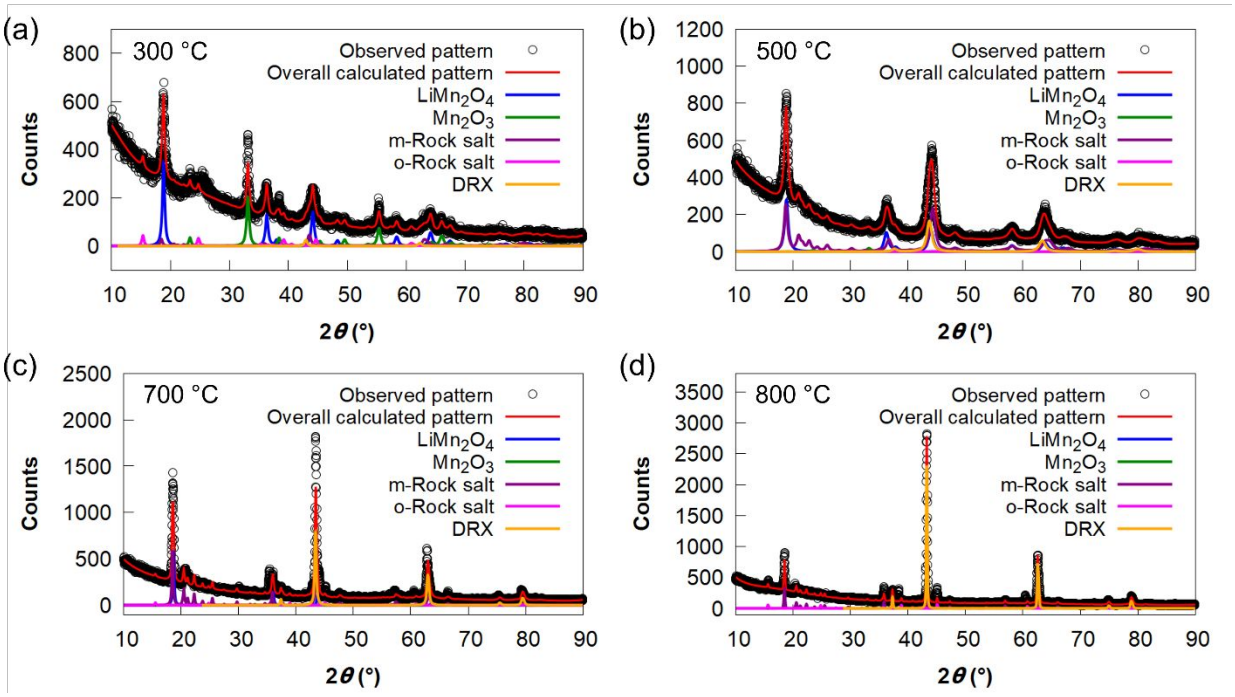

Figure 4 – Rietveld plots of XRD patterns at select temperatures during the *in-situ* synthesis of $Li_{1.25}Mn_{0.5}Ti_{0.3}O_{1.95}F_{0.05}$ (Equation 2). These plots show the observed data, overall calculated pattern, and the patterns arising from each phase (excluding the background). (a) 300 °C, R_{wp} = 10.382%; (b) 500 °C, R_{wp} = 9.268%; (c) 700 °C, R_{wp} = 15.345%; (d) 800 °C, R_{wp} = 11.265%. m-Rock salt and o-Rock salt refer to monoclinic and orthorhombic rock salt phases, respectively.

While the XRD patterns indicate that blending the oxide precursor with LiF is critical to increase DRX phase conversion, these results do not reveal whether F^- anions are successfully incorporated into the DRX lattice, as F^- and O^{2-} possess similar X-ray form factors. To further probe the distribution of local Li and F environments in the final product, the $Li_{1.25}Mn_{0.5}Ti_{0.3}O_{1.95}F_{0.05}$ sample (annealed at 800 °C) was analyzed using ^7Li and ^{19}F solid-state nuclear magnetic resonance (ssNMR) spectroscopy. The ^7Li ssNMR spectrum (see Figure 2c) contains two major components: (i) a sharp resonance near 0 ppm arising from Li in diamagnetic environments (*e.g.*, Li in a Ti^{4+}-only rock salt phase, and/or in amorphous impurities such Li_2CO_3, LiOH, or LiF) and (ii) a broad resonance spanning from –100 to 1000 ppm attributed to Li in the

DRX phase.[29] A shoulder at ~320 ppm indicates the presence of an ordered paramagnetic phase (*e.g.*, monoclinic *m*-$Li_2Mn_{1-x}Ti_xO_3$). Similarly, the signal at ~36 ppm is attributed to orthorhombic $LiMnO_2$ (*o*-$LiMnO_2$),[53] which is consistent with the XRD analysis (Figure 2b). An ordered, monoclinic $LiMnO_2$ phase would have a ^{7}Li resonance at *ca*. 130 – 140 ppm,[53] which is not observed here, and therefore, this phase is not present.

^{19}F ssNMR spectra were recorded under two conditions using either: (i) a long inter-scan delay (20 s) to obtain quantitative insights into the diamagnetic F environments (Figure S3a), or (ii) a short delay (20 ms) to enhance the intensity of fast-relaxing paramagnetic signals (Figure 2d). Notably, ^{19}F ssNMR underestimates the amount of F incorporated into the bulk DRX structure, as F species directly bonded to paramagnetic Mn yield signals that are too short-lived to be observed by NMR. Previous work describes this effect in more detail.[29] A rough fit of the ^{19}F NMR spectrum (Figure S3a) indicates that, while the major component centered at –100 ppm is consistent with F in the DRX phase, a secondary component centered around –200 ppm indicates the presence of a minor, F-containing phase that is too broad to be attributed solely to LiF. To identify this secondary phase, a candidate rock salt phase (Li_3TiO_3F) was synthesized through a solid-state reaction. As shown in Figure S4, XRD and ssNMR measurements indicate this material is phase-pure with a single Li crystallographic environment resonating at 0 ppm and a single F crystallographic site resonating at about –192 ppm. Both chemical shifts are consistent with the impurity signals observed in the ssNMR spectra for $Li_{1.25}Mn_{0.5}Ti_{0.3}O_{1.95}F_{0.05}$ (Figure 2c and Figure 2d). While the ^{19}F resonance for Li_3TiO_3F perfectly matches that of the impurity signal, these phases may contain different F content. Therefore, the impurity is more appropriately described by the general formula $Li_{(2+\delta)/3}Ti_{(1-\delta)/3}O_{1-\delta}F_\delta$, where $\delta > 0$. As $Li_{(2+\delta)/3}Ti_{(1-\delta)/3}O_{1-\delta}F_\delta$ also adopts the *Fm*-3*m* rock salt structure with similar cell parameters to the DRX phase, its presence was not detected by XRD patterns in Figure 2b.

The ssNMR and XRD findings illustrate the importance of using complementary techniques to evaluate phase composition of DRX oxyfluorides. Collectively, these results indicate that $Li_{1.25}Mn_{0.5}Ti_{0.3}O_{1.95}F_{0.05}$ contains a majority DRX phase along with secondary phases including ordered

diamagnetic $Li_{(2+\delta)/3}Ti_{(1-\delta)/3}O_{1-\delta}F_{\delta}$ (^{19}F NMR signal at –193 ppm), paramagnetic Mn-containing (*e.g.*, $Li_2Mn_{1-x}Ti_xO_3$) monoclinic rock salt phases (^{7}Li NMR signal at ~320 ppm), and a small amount of orthorhombic $LiMnO_2$ (^{7}Li signal at ~36 ppm). With the present dataset, we cannot rule out the presence of trace, amorphous impurities, such as Li_2CO_3, LiOH, or LiF.

Additional characterization including SEM and ICP-OES/F-ISE were performed to assess the final products' morphology and overall stoichiometry. Figure 5 shows that $Li_{1.2}Mn_{0.5}Ti_{0.3}O_{1.95}$ and $Li_{1.25}Mn_{0.5}Ti_{0.3}O_{1.95}F_{0.05}$ contain micron-sized primary particles which form large agglomerates (>10 μm). Interestingly, the oxyfluoride sample contains fused grains which may be the result of liquid-phase sintering enabled by a liquid flux (*e.g.*, LiF, T_m= 848°C).[54] Similar grain structure was also observed for the $Li_{1.25}Mn_{0.5}Ti_{0.3}O_{1.95}F_{0.05}$ heated at 800°C (see Figure S5), suggesting the solid-state reaction (Schematic 1, Path C) involves a eutectic containing the oxide precursor, intermediate phases, and/or LiF. As shown in Table S3, oxyfluoride powders heated at 800 and 1000 °C had measured compositions of $Li_{1.25}Mn_{0.36}Ti_{0.41}O_{1.95}F_{0.05}$ and $Li_{1.23}Mn_{0.36}Ti_{0.40}O_{1.95}F_{0.03}$, respectively, indicating minimal Li and F losses occur at 1000 °C. Surprisingly, these samples had a higher-than-expected Mn/Ti ratio. This result is attributed to aging (*i.e.*, partial evaporation) of the Ti-based precursor which increased the effective Ti concentration when preparing the oxide precursor. As such, investigations on Mn-rich DRX cathodes utilized a fresh Ti reagent which was not subject to this error.

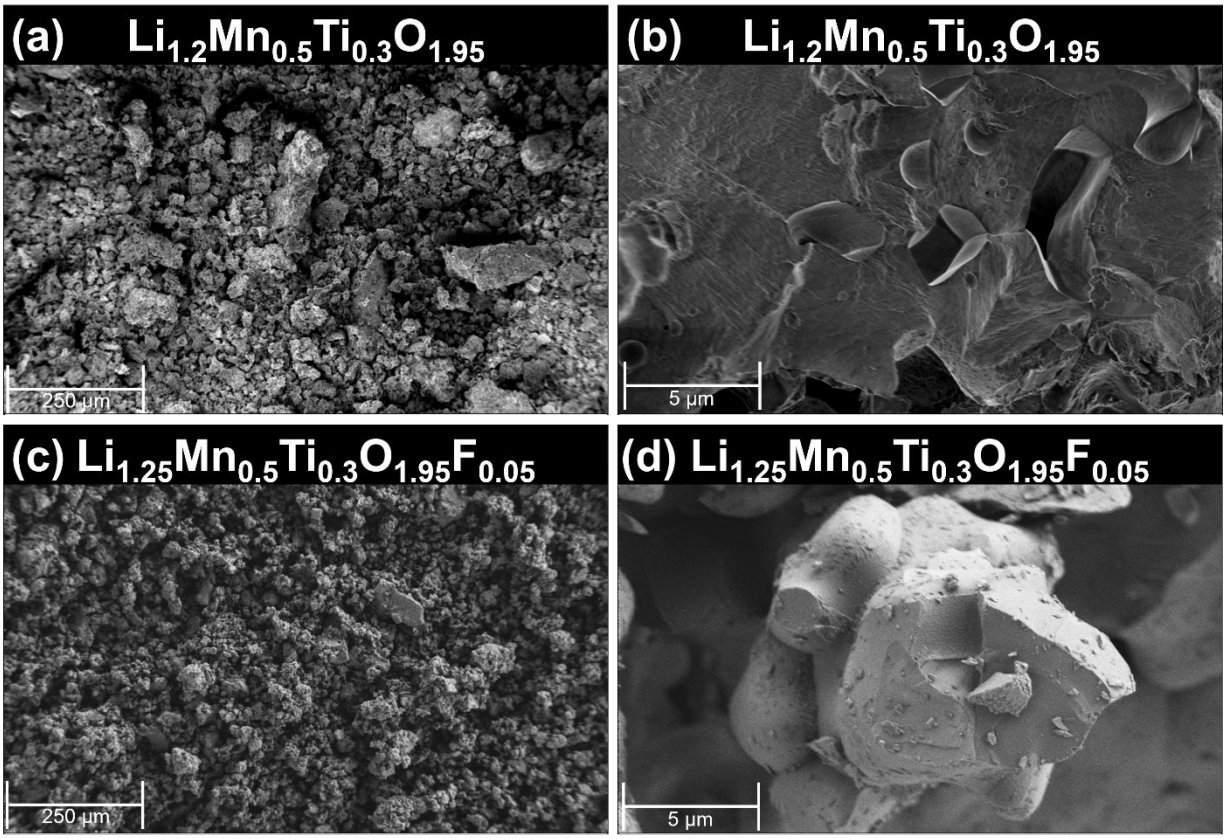

Figure 5 – SEM images of (a) – (b) $Li_{1.2}Mn_{0.5}Ti_{0.3}O_{1.95}$ heated at 1000 °C for 4 h (Schematic 1, Path A) and (c) – (d) $Li_{1.25}Mn_{0.5}Ti_{0.3}O_{1.95}F_{0.05}$ heated at 1000 °C for 1 h (Schematic 1, Path C). All images were collected on as-synthesized DRX powders. Notably, composite cathodes for electrochemical testing were prepared using high-energy ball milling to reduce particle size as described in prior work.[55]

$Li_{1.35}Mn_{0.7}Ti_{0.1}O_{1.85}F_{0.15}$ Oxyfluoride Synthesis

To expand the two-step reaction sequence (Schematic 1) to synthesize Mn-rich DRX cathodes, an oxide precursor with the nominal composition $Li_{1.2}Mn_{0.7}Ti_{0.1}O_{1.85}$ was also prepared (see Figure S1b). Heating the precursor to 1000 °C for 1 h under Ar resulted in monoclinic and orthorhombic ordered rock salt phases with no detectable DRX (Figure 6a). On the other hand, grinding the $Li_{1.2}Mn_{0.7}Ti_{0.1}O_{1.85}$ precursor with LiF (see Equation 3) and annealing under the same conditions yielded predominantly the

desired DRX phase (81.5(8)%, see Figure 6b). The precursor's drying history had negligible impact on the final product (see Table S2).

$$Li_{1.2}Mn_{0.7}Ti_{0.1}O_{1.85} + 0.15LiF \rightarrow Li_{1.35}Mn_{0.7}Ti_{0.1}O_{1.85}F_{0.15} \quad \text{(Equation 3)}$$

Unlike the $Li_{1.25}Mn_{0.5}Ti_{0.3}O_{1.95}F_{0.05}$ sample, the $Li_{1.35}Mn_{0.7}Ti_{0.1}O_{1.85}F_{0.15}$ powder contained a crystalline LiF impurity, which suggests that either: (i) the reaction did not go to completion and/or (ii) the Mn-rich DRX has a lower-than-targeted F^- solubility (see Equation 3). This finding is consistent with previous reports that have shown it is difficult to substitute F^- into Mn-rich DRX materials.[26]

ssNMR was again employed to probe the distribution of Li and F local environments in the $Li_{1.35}Mn_{0.7}Ti_{0.1}O_{1.85}F_{0.15}$ product. The ^{7}Li ssNMR spectrum (Figure 6c) contains a sharp resonance near 0 ppm attributed to Li in diamagnetic impurities (LiF and monoclinic Li_2TiO_3), which were also detected by XRD. The various ^{7}Li signals in the 100 to 1500 ppm region correspond to Li species in paramagnetic environments, including: (i) a very broad resonance spanning 1000 to 0 ppm attributed to Li in the DRX phase[29] and (ii) sharp resonances arising from Li species in ordered rock salt phases. More specifically, the 731 ppm and 1460 ppm signals are assigned to Li in the Li and transition metal layers in monoclinic Li_2MnO_3, and the signal at 131 ppm is assigned to Li in monoclinic $LiMnO_2$.[53, 56, 57] It should be noted that monoclinic $LiMnO_2$ and monoclinic Li_2MnO_3 cannot be readily distinguished by XRD. Two additional resonances are observed at ~528 ppm and 1220 ppm, which are attributed to Li in a monoclinic $Li_2Mn_{1-x}Ti_xO_3$ phase, where partial substitution of Mn by Ti reduces the ^{7}Li chemical shifts compared to that of Li_2MnO_3.

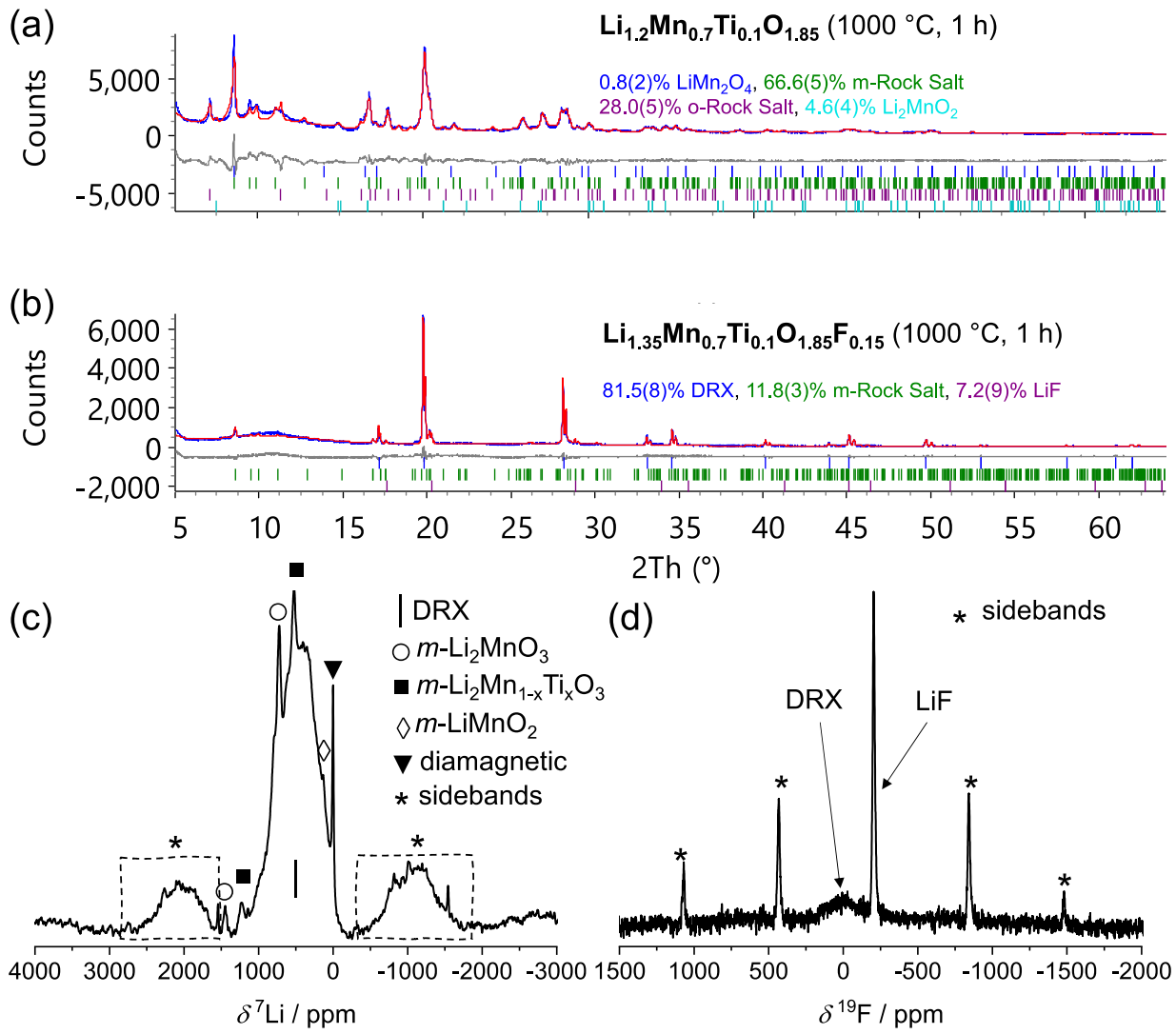

Figure 6 – (a–b) Rietveld plots (Mo radiation) of the product obtained from heating $Li_{1.2}Mn_{0.7}Ti_{0.1}O_{1.85}$ at 1000 °C for 1 h (a) without LiF (Schematic 1, Path A), R_{wp} = 12.655%, χ^2 = 3.641 and (b) with LiF (Schematic 1, Path C and Equation 3) to yield $Li_{1.35}Mn_{0.7}Ti_{0.1}O_{1.85}F_{0.15}$, R_{wp} = 13.107%, χ^2 = 2.020. Blue curves = observed data; red curves = calculated pattern; grey curves = difference between observed and calculated. Tick marks correspond to reflections arising from each phase. m-Rock Salt and o-Rock Salt refer to monoclinic and orthorhombic rock salt phases, respectively. (c–d) ssNMR results for $Li_{1.35}Mn_{0.7}Ti_{0.1}O_{1.85}F_{0.15}$ including (c) ^{7}Li (D1 = 20s) and (d) ^{19}F (D1 = 20 ms) spectra. Side bands are denoted with asterisks (*). ssNMR spectra were obtained at a 100 MHz field and at 40 kHz magic angle spinning (MAS).

The ^{19}F ssNMR spectrum collected on $Li_{1.35}Mn_{0.7}Ti_{0.1}O_{1.85}F_{0.15}$ is shown in Figure 6d. The sharp resonance at *ca*. –204 ppm is assigned to LiF, while the broad resonance spanning 270 to –380 ppm is attributed to F in the DRX phase.[58] A fit of the data (Figure S3b) indicates at least 42% of the F was incorporated into the DRX structure. Overall, these results demonstrate that the synthesis route reported herein is viable to produce DRX oxyfluorides without the need for high-energy ball milling.

The morphologies of $Li_{1.2}Mn_{0.7}Ti_{0.1}O_{1.85}$ and $Li_{1.35}Mn_{0.7}Ti_{0.1}O_{1.85}F_{0.15}$ were assessed using SEM as shown in Figure 7. Both samples contain micron-sized agglomerates similar to $Li_{1.2}Mn_{0.5}Ti_{0.3}O_{1.95}$ and $Li_{1.25}Mn_{0.5}Ti_{0.3}O_{1.95}F_{0.05}$ (Figure 5). While not a primary focus of the current work, modifying the solution composition is anticipated to enable one to control the DRX particle morphology. For example, the fuel-to-oxidizer ratio in combustion reactions often has a dramatic impact on particle shape, size, and agglomeration.[42, 59] These morphological variations are largely influenced by differences in heat released and gas evolution during the exothermic reaction. Such investigations are recommended for future work on DRX cathodes prepared using this route.

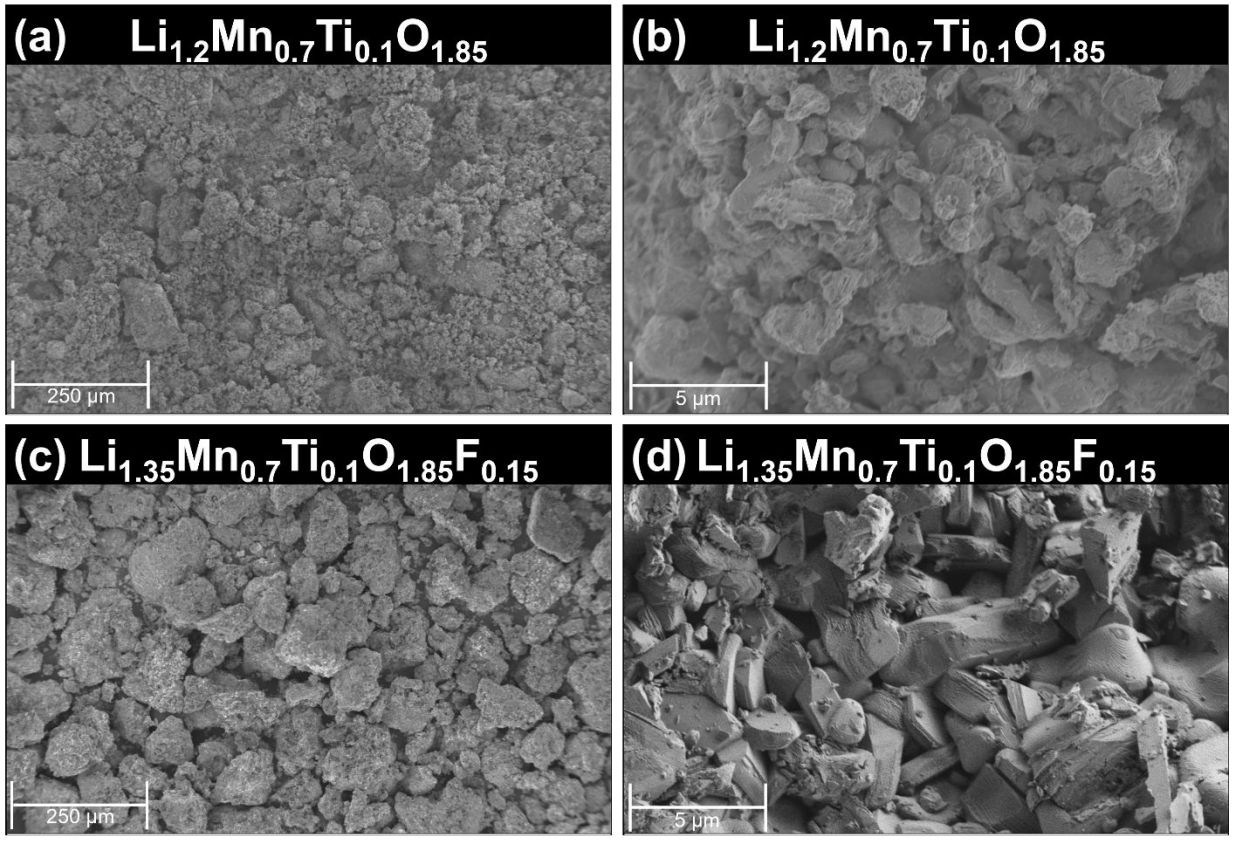

Figure 7 – SEM images of (a) – (b) $Li_{1.2}Mn_{0.7}Ti_{0.1}O_{1.85}$ (Schematic 1, Path A) and (c) – (d) $Li_{1.35}Mn_{0.7}Ti_{0.1}O_{1.85}F_{0.15}$ (Schematic 1, Path C). All images were collected on as-synthesized DRX powders prepared by heating at 1000 °C for 1 h. Notably, composite electrodes for electrochemical testing were prepared using high-energy ball milling to reduce particle size as described in prior work.[55]

For the oxyfluoride sample, ICP-OES/F-ISE results indicate an overall composition of $Li_{1.26}Mn_{0.72}Ti_{0.11}O_{1.85}F_{0.15}$ (see Table S3), which is in good agreement with the nominal stoichiometry ($Li_{1.35}Mn_{0.7}Ti_{0.1}O_{1.85}F_{0.15}$). The product's slight Li deficiency ($Li_{1.26}$ *versus* $Li_{1.35}$) suggests some Li loss occurs during either the combustion reaction or high-temperature annealing step. As such, the effect of lower annealing temperatures was also investigated as shown in Figure S2d. Heating $Li_{1.2}Mn_{0.7}Ti_{0.1}O_{1.85}$ with LiF at 800 °C for 1 h resulted in only 12.6(7)% DRX, compared to 92.0(2)% DRX for $Li_{1.25}Mn_{0.5}Ti_{0.3}O_{1.95}F_{0.05}$ heated under the same conditions (Figure S2b). The need for higher reaction

temperatures to produce Mn-rich DRX powders has also been reported in previous studies.[10, 26] The increased difficulty in forming these phases may be related to the stability of the ordered rock salt Li_2MnO_3, for which an order-disorder transition has not been reported.[20] To address the moderate DRX purity in the present study, future work is recommended to explore alternative precursor designs (*e.g.*, altering the Li and/or vacancy content) which may influence the reaction pathway and product's structure.

Electrochemical Characterization

The electrochemical properties of DRX oxyfluorides were evaluated in Li metal half cells (see Figure 8). Composite cathodes were prepared in a two-step process where: (i) high energy milling was used to coat the active material with graphite (78:22 w:w) followed by (ii) slurry mixing and electrode casting. As described in previous work,[55] graphite is a preferable conductive additive due to formation of a robust electronically conductive network and a more stable cathode/electrolyte interface. During the first cycle, the $Li_{1.35}Mn_{0.7}Ti_{0.1}O_{1.85}F_{0.15}$ cathode had a high charge capacity of 274 mAh g^{-1} and reversible capacity of 209 mAh g^{-1}, corresponding to an initial coulombic efficiency of 76%. Interestingly, the cathode with lower Mn content ($Li_{1.25}Mn_{0.5}Ti_{0.3}O_{1.95}F_{0.05}$) had slightly higher capacity (see Figure S7), which is attributed to the sample's higher DRX purity. These results indicate charge compensation occurs through Mn and O redox centers as expected.[7, 18, 60] In general, the performance of Mn/Ti-based DRX cathodes is highly dependent on the Mn content and processing history. For example, materials prepared through sol-gel[7], mechanochemical,[61] and solid-state[62] reactions have been reported with initial reversible capacities ranging from approximately 200 – 250 mAh g^{-1}. For a more detailed discussion on the topic, we refer to a comprehensive review by Li *et al*.[63]

While the initial cycles showed a sloping voltage profile, extended cycling of $Li_{1.35}Mn_{0.7}Ti_{0.1}O_{1.85}F_{0.15}$ yielded a plateau ~3 V *vs*. Li/Li^+ due to formation of a spinel-like δ phase which is well-known for Mn-rich DRX cathodes.[19, 64] The material also showed good cycling stability with 65% capacity retention after 150 cycles. Capacity fade in these cells is primarily attributed to an unstable

cathode/electrolyte interface due to electrolyte breakdown at high states of charge. This effect is also illustrated by the moderate coulombic efficiency ~95% during extended cycling (Figure 8b) which is a result of parasitic reactions occurring at both the DRX cathode and Li metal anode. As recently reported for $Li_{1.2}Mn_{0.5}Ti_{0.3}O_{1.9}F_{0.1}$, catalytic decomposition of the electrolyte is heavily influenced by the conductive additive's structure, surface area, and loading.[55] While efforts to optimize the cathode/electrolyte interface are outside the present study's scope, the results in Figure 8 demonstrate that cathodes derived from a combustion reaction have reproducible and competitive performance with materials obtained through traditional solid-state reactions.[7] Ongoing work is aimed at fine-tuning the synthesis conditions (*e.g.*, to eliminate secondary phases such as $LiMnO_2$ that may be electrochemically active), which is anticipated to further improve the cathode's performance.

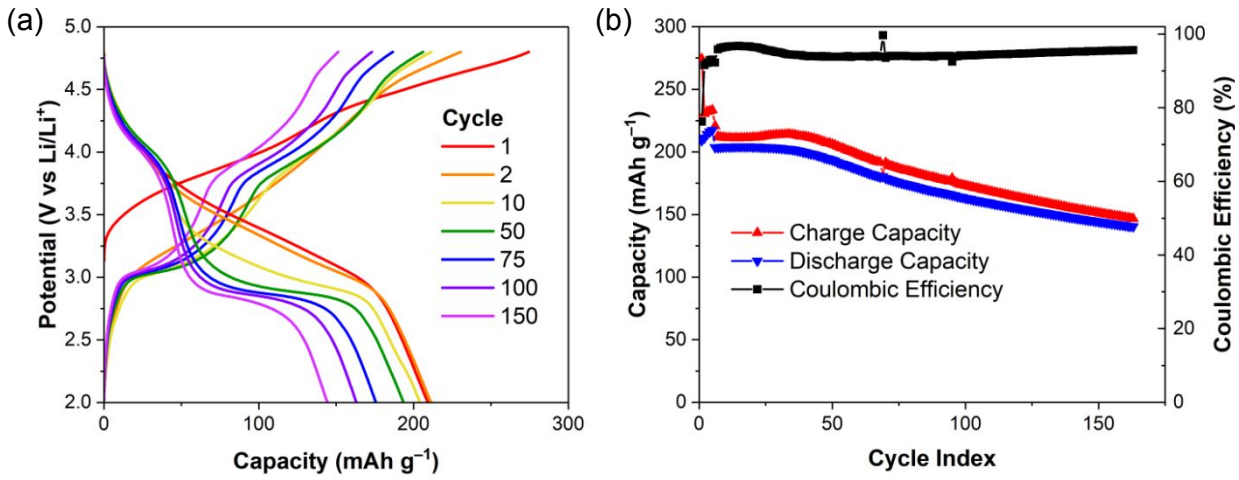

Figure 8 – (a) Galvanostatic voltage profiles and (b) cycling stability of a $Li_{1.35}Mn_{0.7}Ti_{0.1}O_{1.85}F_{0.15}$ DRX cathode. The cathode was cycled against a Li metal reference/counter electrode between 2.0 V and 4.8 V at a specific current of 10 mA g^{-1} for the first 5 cycles and 20 mA g^{-1} for subsequent cycles.

Conclusions

The present work reports a new synthesis route to prepare high-performance Mn/Ti-based DRX oxyfluoride cathodes. A two-step reaction sequence was developed where a combustion reaction was used to prepare a lithiated metal oxide precursor followed by high-temperature reactions at 800 – 1000 °C. Annealing the oxide precursor yields undesired ordered rock salt and spinel phases, but mixing the precursor with LiF facilitates DRX formation and increases the powder's phase purity up to 90%. Furthermore, the synthesis route reported herein enables DRX formation at lower temperatures and/or shorter times compared to conventional solid-state methods, which are difficult to scale. More specifically, high DRX phase conversion was obtained after 1 h reactions at 800 °C and 1000 °C for $Li_{1.25}Mn_{0.5}Ti_{0.1}O_{1.95}F_{0.05}$ and $Li_{1.35}Mn_{0.7}Ti_{0.1}O_{1.85}F_{0.15}$, respectively. These findings were complemented by *in-situ* XRD measurements to investigate the reaction pathway and intermediate phases formed. Additionally, ^{7}Li- and ^{19}F-ssNMR measurements demonstrate that F^- was successfully incorporated into the DRX anion sublattice.

Mn-rich oxyfluoride DRX cathodes prepared using this route showed promising electrochemical performance with reversible capacities ~210 mAh g^{-1} and good cycling stability in half cells. These results are competitive with similar DRX formulations prepared using conventional solid-state routes. Future investigations are recommended to optimize other reaction parameters (*e.g.*, fuel content/composition, precursor stoichiometry, thermal quenching rate, and F content) to maximize yield of the desired oxyfluoride phase and control particle morphology. Beyond energy storage applications, this synthesis approach can also be used to prepare other metastable phases not accessible through traditional routes.

Conflicts of Interest

The corresponding authors (M. S. Chambers, E. C. Self and B. L. Armstrong) have filed a US Provisional Patent Application Serial No. 63/715,138 for combustion synthesis of DRX cathode materials reported in this manuscript.

Data Availability Statement

The data used to support the findings of this study are included within the article.

Acknowledgements

The authors would like to thank Khryslyn Araño and Ji-young Ock of the Oak Ridge National Laboratory for providing advice with casting electrodes and aiding with coin cell assembly, respectively. The authors would also like to thank Gabriel Veith of the Oak Ridge National Laboratory for providing mentorship and supervision to Matthew S. Chambers. Research conducted at Oak Ridge National Laboratory, managed by UT Battelle, LLC, for the US Department of Energy (DOE) was sponsored by the Vehicle Technologies Office (VTO) under the Office of Energy Efficiency and Renewable Energy (EERE). Research conducted at UC Santa Barbara was supported by the Assistant Secretary for Energy Efficiency and Renewable Energy, Vehicle Technologies Office under the Applied Battery Materials Program of the US Department of Energy (DOE) under contract number DE-AC02-05CH11231 (DRX+). This work made use of the MRL MRSEC Spectroscopy Facility at UC Santa Barbara (DMR–2308708), a member of the Materials Research Facilities Network (https://www.mrfn.org).

This manuscript has been authored in part by UT-Battelle, LLC, under contract DE-AC05–00OR22725 with the US Department of Energy (DOE). The publisher, by accepting the article for

References

1. M. S. Islam, D. J. Driscoll, C. A. J. Fisher and P. R. Slater, Atomic-Scale Investigation of Defects, Dopants, and Lithium Transport in the $LiFePO_4$ Olivine-Type Battery Material, *Chemistry of Materials*, 2005, **17**, 5085-5092.
2. Y. Wang, E. Wang, X. Zhang and H. Yu, High-Voltage "Single-Crystal" Cathode Materials for Lithium-Ion Batteries, *Energy & Fuels*, 2021, **35**, 1918-1932.
3. H. Cai, R. Chen, M. Bahri, C. J. Hawkins, M. Sonni, L. M. Daniels, J. Lim, J. A. Evans, M. Zanella, L. A. H. Jones, T. D. Manning, T. D. Veal, L. J. Hardwick, M. S. Dyer, N. D. Browning, J. B. Claridge and M. J. Rosseinsky, Fluorine-Rich Oxyfluoride Spinel-like $Li_{1.25}Ni_{0.625}Mn_{1.125}O_3F$ Utilizing Redox-Active Ni and Mn for High Capacity and Improved Cyclability, *ACS Materials Letters*, 2023, DOI: 10.1021/acsmaterialslett.2c00973, 527-535.
4. S. Jiao, J. Wang, Y.-S. Hu, X. Yu and H. Li, High-Capacity Oxide Cathode beyond 300 mAh/g, *ACS Energy Letters*, 2023, **8**, 3025-3037.
5. K. Kawai, T. Sudayama, D. Asakura, J. Kikkawa, E. Watanabe, M. Okubo and A. Yamada, High-Voltage Electrochemical Properties of Lithium-Rich Spinel Oxides, *The Journal of Physical Chemistry C*, 2023, DOI: 10.1021/acs.jpcc.3c01184.
6. J. Wang, Y. Xu, Y. Niu, Y. Liu and X. Yao, Lithium-Ion Conductivity Epitaxial Layer Contributing to the Structure and Cycling Stability of $LiMn_2O_4$ Cathodes, *ACS Sustainable Chemistry & Engineering*, 2023, DOI: 10.1021/acssuschemeng.2c06738.
7. S. Patil, D. Darbar, E. C. Self, T. Malkowski, V. C. Wu, R. Giovine, N. J. Szymanski, R. D. McAuliffe, B. Jiang, J. K. Keum, K. P. Koirala, B. Ouyang, K. Page, C. Wang, G. Ceder, R. J. Clément and J. Nanda, Alternate Synthesis Method for High-Performance Manganese Rich Cation Disordered Rocksalt Cathodes, *Advanced Energy Materials*, 2022, **n/a**, 2203207.
8. I. Blumenhofer, Y. Shirazi Moghadam, A. El Kharbachi, Y. Hu, K. Wang and M. Fichtner, Synthesis and Structure Stabilization of Disordered Rock Salt Mn/V-Based Oxyfluorides as Cathode Materials for Li-Ion Batteries, *ACS Materials Au*, 2022, DOI: 10.1021/acsmaterialsau.2c00064.
9. J. Lee, A. Urban, X. Li, D. Su, G. Hautier and G. Ceder, Unlocking the Potential of Cation-Disordered Oxides for Rechargeable Lithium Batteries, *Science*, 2014, **343**, 519-522.
10. N. J. Szymanski, Y. Zeng, T. Bennett, S. Patil, J. K. Keum, E. C. Self, J. Bai, Z. Cai, R. Giovine, B. Ouyang, F. Wang, C. J. Bartel, R. J. Clément, W. Tong, J. Nanda and G. Ceder, Understanding the Fluorination of Disordered Rocksalt Cathodes through Rational Exploration of Synthesis Pathways, *Chemistry of Materials*, 2022, **34**, 7015-7028.
11. X. Guo, C. Chen and S. P. Ong, Intercalation Chemistry of the Disordered Rocksalt $Li_3V_2O_5$ Anode from Cluster Expansions and Machine Learning Interatomic Potentials, *Chemistry of Materials*, 2023, DOI: 10.1021/acs.chemmater.2c02839.
12. M. J. A. Leesmith, N. R. Halcovitch and X. Hua, Electrochemical lithiation-induced formation of disordered rocksalt, *Journal of Materials Chemistry A*, 2023, DOI: 10.1039/D3TA01740K.

13. N. J. Szymanski, Z. Lun, J. Liu, E. C. Self, C. J. Bartel, J. Nanda, B. Ouyang and G. Ceder, Modeling Short-Range Order in Disordered Rocksalt Cathodes by Pair Distribution Function Analysis, *Chemistry of Materials*, 2023, **35**, 4922-4934.
14. Y. Sun, S. Jiao, J. Wang, Y. Zhang, J. Liu, X. Wang, L. Kang, X. Yu, H. Li, L. Chen and X. Huang, Expandable Li Percolation Network: The Effects of Site Distortion in Cation-Disordered Rock-Salt Cathode Material, *Journal of the American Chemical Society*, 2023, **145**, 11717-11726.
15. V. C. Wu, H. A. Evans, R. Giovine, M. B. Preefer, J. Ong, E. Yoshida, P.-E. Cabelguen and R. J. Clément, Rapid and Energy-Efficient Synthesis of Disordered Rocksalt Cathodes, *Advanced Energy Materials*, 2023, **13**, 2203860.
16. H. Ji, A. Urban, D. A. Kitchaev, D.-H. Kwon, N. Artrith, C. Ophus, W. Huang, Z. Cai, T. Shi, J. C. Kim, H. Kim and G. Ceder, Hidden structural and chemical order controls lithium transport in cation-disordered oxides for rechargeable batteries, *Nature Communications*, 2019, **10**, 592.
17. X. Fan, Q. Qin, D. Liu, A. Dou, M. Su, Y. Liu and J. Pan, Synthesis and electrochemical performance of Li_3NbO_4-based cation-disordered rock-salt cathode materials for Li-ion batteries, *Journal of Alloys and Compounds*, 2019, **797**, 961-969.
18. J. Lee, D. A. Kitchaev, D.-H. Kwon, C.-W. Lee, J. K. Papp, Y.-S. Liu, Z. Lun, R. J. Clément, T. Shi, B. D. McCloskey, J. Guo, M. Balasubramanian and G. Ceder, Reversible Mn^{2+}/Mn^{4+} double redox in lithium-excess cathode materials, *Nature*, 2018, **556**, 185-190.
19. J. Ahn, R. Giovine, V. C. Wu, K. P. Koirala, C. Wang, R. J. Clément and G. Chen, Ultrahigh-Capacity Rocksalt Cathodes Enabled by Cycling-Activated Structural Changes, *Advanced Energy Materials*, 2023, **13**, 2300221.
20. X. Zhi and A. R. West, Mechanosynthesis of Disordered Rock Salt Structures: Thermodynamic and Kinetic Considerations, *Chemistry of Materials*, 2023, DOI: 10.1021/acs.chemmater.3c01080.
21. Q. Deville, R. Wernert, V. Dillay, B. Mortemard de Boisse, M. Guignard and D. Carlier, Influence of Synthesis Parameters on the Short-Range Structure and Electrochemical Performances of Li_2MnO_2F, *Inorganic Chemistry*, 2024, DOI: 10.1021/acs.inorgchem.3c03863.
22. I. Roy, K. Kumar, H. Li, N. Sunariwal, G. C. B. Alexander, J. W. Freeland, F. Rodolakis and J. Cabana, Activity of Metal-Fluorine States upon Delithiation of Disordered Rocksalt Oxyfluorides, *Chemistry of Materials*, 2023, DOI: 10.1021/acs.chemmater.2c03680.
23. L. L. Driscoll, E. H. Driscoll, B. Dong, F. N. Sayed, J. N. Wilson, C. A. O'Keefe, D. J. Gardner, C. P. Grey, P. K. Allan, A. A. L. Michalchuk and P. R. Slater, Under pressure: offering fundamental insight into structural changes on ball milling battery materials, *Energy & Environmental Science*, 2023, **16**, 5196-5209.
24. A. Kanno, Y. Ugata, I. Ikeuchi, M. Hibino, K. Nakura, Y. Miyaoka, I. Kawamura, D. Shibata, T. Ohta and N. Yabuuchi, Durable Manganese-Based Li-Excess Electrode Material without Voltage Decay: Metastable and Nanosized $Li_2MnO_{1.5}F_{1.5}$, *ACS Energy Letters*, 2023, **8**, 2753-2761.
25. Y. Shirazi Moghadam, A. El Kharbachi, T. Diemant, G. Melinte, Y. Hu and M. Fichtner, Toward Better Stability and Reversibility of the Mn^{4+}/Mn^{2+} Double Redox Activity in Disordered Rocksalt Oxyfluoride Cathode Materials, *Chemistry of Materials*, 2021, **33**, 8235-8247.
26. V. C. Wu, P. Zhong, J. Ong, E. Yoshida, A. Kwon, G. Ceder and R. J. Clément, The Limited Incorporation and Role of Fluorine in Mn-rich Disordered Rocksalt Cathodes, *ACS Energy Letters*, 2024, DOI: 10.1021/acsenergylett.4c01075, 3027-3035.
27. S. Jiao, Y. Sun, J. Wang, D. Shi, Y. Li, X. Jiang, F. Wang, Y. Zhang, J. Liu, X. Wang, X. Yu, H. Li, L. Chen and X. Huang, The Mechanism of Fluorine Doping for the Enhanced Lithium Storage Behavior in Cation-Disordered Cathode Oxide, *Advanced Energy Materials*, 2023, 2301636.
28. B. Ouyang, N. Artrith, Z. Lun, Z. Jadidi, D. A. Kitchaev, H. Ji, A. Urban and G. Ceder, Effect of Fluorination on Lithium Transport and Short-Range Order in Disordered-Rocksalt-Type Lithium-Ion Battery Cathodes, *Advanced Energy Materials*, 2020, **10**, 1903240.
29. R. Giovine, E. Yoshida, V. C. Wu, Y. Ji, M. J. Crafton, B. D. McCloskey and R. J. Clément, An Experimental Approach to Assess Fluorine Incorporation into Disordered Rock Salt Oxide Cathodes, *Chemistry of Materials*, 2024, **36**, 3643-3654.

30. W. D. Richards, S. T. Dacek, D. A. Kitchaev and G. Ceder, Fluorination of Lithium-Excess Transition Metal Oxide Cathode Materials, *Advanced Energy Materials*, 2018, **8**, 1701533.
31. D. Chen, J. Zhang, Z. Jiang, C. Wei, J. Burns, L. Li, C. Wang, K. Persson, Y. Liu and G. Chen, Role of Fluorine in Chemomechanics of Cation-Disordered Rocksalt Cathodes, *Chemistry of Materials*, 2021, **33**, 7028-7038.
32. F. Kalyk, A. Stankevičiūtė, G. Budrytė, G. Gaidamavičienė, A. Žalga, R. Kriūkienė, Ž. Kavaliauskas, M. Leszczyńska and B. Abakevičienė, Comparative study of samarium-doped ceria nanopowders synthesized by various chemical synthesis routes, *Ceramics International*, 2020, **46**, 24385-24394.
33. C. Aliotta, L. F. Liotta, V. La Parola, A. Martorana, E. N. S. Muccillo, R. Muccillo and F. Deganello, Ceria-based electrolytes prepared by solution combustion synthesis: The role of fuel on the materials properties, *Applied Catalysis B: Environmental*, 2016, **197**, 14-22.
34. T. Saradha, A. Subramania, K. Balakrishnan and S. Muzhumathi, Microwave-assisted combustion synthesis of nanocrystalline Sm-doped $La_2Mo_2O_9$ oxide-ion conductors for SOFC application, *Materials Research Bulletin*, 2015, **68**, 320-325.
35. P. K. Dager, C. M. Chanquía, L. Mogni and A. Caneiro, Synthesis of pure-phase Sr_2MgMoO_6 nanostructured powder by the combustion method, *Materials Letters*, 2015, **141**, 248-251.
36. T. Changan, L. Junliang, G. Cuijing, C. Jun, C. Tongxiang and Z. Yanwei, Auto-combustion synthesis of apatite-type $La_{9.33}Ge_6O_{26}$ ultrafine powder and its characterization, *Journal of Alloys and Compounds*, 2008, **460**, 646-650.
37. S. Saha, S. J. Ghanawat and R. D. Purohit, Solution combustion synthesis of nano particle $La_{0.9}Sr_{0.1}MnO_3$ powder by a unique oxidant-fuel combination and its characterization, *Journal of Materials Science*, 2006, **41**, 1939-1943.
38. C. O. Ehi-Eromosele, S. O. Ajayi and C. N. Onwucha, Optimizing the electrochemical performance of Li2MnO3 cathode materials for Li-ion battery using solution combustion synthesis: Higher temperature and longer syntheses improves performance, *J. Alloys Compd.*, 2021, **861**, 157972.
39. C. U. Mulik, R. S. Kamat, X. Wang, C. Padwal, M. Y. Chougale, D. P. Dubal and L. D. Jadhav, High-performance Li-ion battery cathode: Mn-doped LiFePO4 via solution combustion synthesis method, *J. Electroanal. Chem.*, 2024, **971**, 118568.
40. S. Wang, M. Xiang, Y. Lu, J. Guo, C. Su, H. Bai and X. Liu, Facile solid-state combustion synthesis of Al–Ni dual-doped LiMn2O4 cathode materials, *Journal of Materials Science: Materials in Electronics*, 2020, **31**, 6036-6044.
41. W. Yang, G. Zhang, J. Xie, L. Yang and Q. Liu, A combustion method to prepare spinel phase LiMn2O4 cathode materials for lithium-ion batteries, *J. Power Sources*, 1999, **81-82**, 412-415.
42. B. L. Armstrong, Consolidation of Nano-Crystalline ZrO_2, *Materials and Manufacturing Processes*, 1996, **11**, 999-1012.
43. A. Rawat, L. Clark, C. Zhang, J. Cavin, V. K. Sangwan, P. S. Toth, C. Janáky, R. Ananth, E. Goldfine, M. J. Bedzyk, E. A. Weiss, J. M. Rondinelli, M. C. Hersam, E. I. Meletis and K. Rajeshwar, Solution Combustion Synthesis and Characterization of Magnesium Copper Vanadates, *Inorganic Chemistry*, 2023, DOI: 10.1021/acs.inorgchem.3c00452.
44. T. d. S. Haas, W. L. de Almeida, F. A. L. Sánchez and V. C. de Sousa, Perovskites used as cathode in solid oxide fuel cells synthesized by solution combustion synthesis (SCS), *Journal of Materials Science: Materials in Electronics*, 2023, **34**, 1530.
45. A. Mao, H.-Z. Xiang, Z.-G. Zhang, K. Kuramoto, H. Yu and S. Ran, Solution combustion synthesis and magnetic property of rock-salt (Co0.2Cu0.2Mg0.2Ni0.2Zn0.2)O high-entropy oxide nanocrystalline powder, *J. Magn. Magn. Mater.*, 2019, **484**, 245-252.
46. L. A. Chick, L. R. Pederson, G. D. Maupin, J. L. Bates, L. E. Thomas and G. J. Exarhos, Glycine-nitrate combustion synthesis of oxide ceramic powders, *Materials Letters*, 1990, **10**, 6-12.
47. H. Rietveld, A profile refinement method for nuclear and magnetic structures, *Journal of Applied Crystallography*, 1969, **2**, 65-71.

48. A. A. Coelho, J. Evans, I. Evans, A. Kern and S. Parsons, The TOPAS symbolic computation system, *Powder Diffraction*, 2011, **26**, S22-S25.
49. K. Mukai, M. Yashima, K. Hibino and T. Terai, Experimental Visualization of Interstitialcy Diffusion of Li Ion in β-Li_2TiO_3, *ACS Applied Energy Materials*, 2019, **2**, 5481-5489.
50. A. Boulineau, L. Croguennec, C. Delmas and F. Weill, Structure of Li_2MnO_3 with different degrees of defects, *Solid State Ionics*, 2010, **180**, 1652-1659.
51. L. Croguennec, P. Deniard, R. Brec and A. Lecerf, Preparation, physical and structural characterization of $LiMnO_2$ samples with variable cationic disorder, *Journal of Materials Chemistry*, 1995, **5**, 1919-1925.
52. A. A. Voskanyan and K. Y. Chan, Kilogram-scale fabrication of 3D CeO_2 active catalytic support with tailored 12 nm spherical mesopores via colloidal solution combustion synthesis, *Microporous and Mesoporous Materials*, 2019, **286**, 182-186.
53. C. P. Grey and N. Dupré, NMR Studies of Cathode Materials for Lithium-Ion Rechargeable Batteries, *Chemical Reviews*, 2004, **104**, 4493-4512.
54. O.-H. Kwon and G. L. Messing, Kinetic Analysis of Solution-Precipitation During Liquid-Phase Sintering of Alumina, *Journal of the American Ceramic Society*, 1990, **73**, 275-281.
55. S. Patil, K. P. Koirala, M. J. Crafton, G. Yang, W. Y. Tsai, B. D. McCloskey, C. Wang, J. Nanda and E. C. Self, Enhanced Electrochemical Performance of Disordered Rocksalt Cathodes Enabled by a Graphite Conductive Additive, *ACS Appl. Mater. Interfaces*, 2023, **15**, 39253-39264.
56. F. Dogan, J. R. Croy, M. Balasubramanian, M. D. Slater, H. Iddir, C. S. Johnson, J. T. Vaughey and B. Key, Solid State NMR Studies of Li_2MnO_3 and Li-Rich Cathode Materials: Proton Insertion, Local Structure, and Voltage Fade, *Journal of The Electrochemical Society*, 2015, **162**, A235.
57. Y. J. Lee, F. Wang and C. P. Grey, ^6Li and ^7Li MAS NMR Studies of Lithium Manganate Cathode Materials, *Journal of the American Chemical Society*, 1998, **120**, 12601-12613.
58. T. Li, T. S. Geraci, K. P. Koirala, A. Zohar, E. N. Bassey, P. A. Chater, C. Wang, A. Navrotsky and R. J. Clément, Structural Evolution in Disordered Rock Salt Cathodes, *Journal of the American Chemical Society*, 2024, DOI: 10.1021/jacs.4c04639.
59. E. Novitskaya, J. P. Kelly, S. Bhaduri and O. A. Graeve, A review of solution combustion synthesis: an analysis of parameters controlling powder characteristics, *Int. Mater. Rev.*, 2020, **66**, 188-214.
60. J. Ahn, D. Chen and G. Chen, A Fluorination Method for Improving Cation-Disordered Rocksalt Cathode Performance, *Advanced Energy Materials*, 2020, **10**, 2001671.
61. Y. Shirazi Moghadam, S. Dinda, A. El Kharbachi, G. Melinte, C. Kübel and M. Fichtner, Structural and Electrochemical Insights from the Fluorination of Disordered Mn-Based Rock Salt Cathode Materials, *Chem. Mater.*, 2022, **34**, 2268-2281.
62. K. Zhou, S. Zheng, H. Liu, C. Zhang, H. Gao, M. Luo, N. Xu, Y. Xiang, X. Liu, G. Zhong and Y. Yang, Elucidating and Mitigating the Degradation of Cationic-Anionic Redox Processes in Li(1.2)Mn(0.4)Ti(0.4)O(2) Cation-Disordered Cathode Materials, *ACS Appl. Mater. Interfaces*, 2019, **11**, 45674-45682.
63. H. Li, R. Fong, M. Woo, H. Ahmed, D.-H. Seo, R. Malik and J. Lee, Toward high-energy Mn-based disordered-rocksalt Li-ion cathodes, *Joule*, 2022, **6**, 53-91.
64. Z. Cai, B. Ouyang, H.-M. Hau, T. Chen, R. Giovine, K. P. Koirala, L. Li, H. Ji, Y. Ha, Y. Sun, J. Huang, Y. Chen, V. Wu, W. Yang, C. Wang, R. J. Clément, Z. Lun and G. Ceder, In situ formed partially disordered phases as earth-abundant Mn-rich cathode materials, *Nature Energy*, 2024, **9**, 27-36.

Data Availability Statement

The data used to support the findings of this study are included within the article.